The shear behaviour of non-prismatic reinforced concrete beams determined using digital image correlation

J J Orr[a], A P Darby[a], T J Ibell[a], M Evernden[a], P Lava[b] and D Debruyne[b]

Abstract

It can be seen that when subject to a uniformly distributed load, a prismatic, steel reinforced concrete beam with constant longitudinal and transverse reinforcement percentages is inefficient. Following simple optimisation routines can result in beams whose flexural and shear capacities reflect the requirements of their loading envelope, and such elements tend to be non-prismatic. Structural research into the use of flexible formwork has developed simple methods for the creation of such elements to offer material and embodied carbon savings of up to 40%.

However, the shear behaviour of such variable section steel reinforced concrete beams has previously been an area of confusion for designers, who must often rely on empirical relationships derived from prismatic beam tests. This paper presents the results of new tests undertaken at the University of Bath on tapered concrete beams designed using BS EN 1992-1-1 [1], the compressive force path method and a strut and tie model, in which digital image correlation was used to analyse the specimens.

Using the 'MatchID' program, strain distributions in each of the specimens during loading were determined, with the results allowing important comparisons to be drawn between the various design methods. A digital image correlation (DIC) technique was subsequently used to verify new proposals for the shear design of non-prismatic concrete beams, which aim to provide improved guidance for designers of optimised concrete structures.

Contact information

[a] j.j.orr@bath.ac.uk
Department of Architecture and Civil Engineering
University of Bath, Bath BA2 7AY
[b] pascal.lava@kahosl.be
Department of Mechanical Engineering
Catholic University College Ghent, B-9000 Ghent, Belgium

Introduction

The manufacture of cement, the principle component of our most widely used man-made material, is estimated to account for some 5% of global carbon dioxide emissions [2]. In the UK, as much as half of all carbon emissions are attributable to the built environment [3], putting a new incentive on designers for the creation of low-carbon, optimised structures. Yet in the case of concrete, recent research has shown that as much as 40% of the structural material in a typical office building could have been omitted if simple optimisation processes had been followed during the design stage [4].

This carbon intensive approach has precipitated research into optimisation methods for concrete structures, where it is apparent that whilst conventional concrete structures tend to be prismatic, optimised structures tend to be quite the opposite. In fact, their shape, being defined by envelope of loads applied to them, can be considerably more complex than is found in traditional construction. The widespread use of optimised concrete structures, which offer immediate opportunities for reductions in embodied carbon, may previously have been hampered by two factors. First, the behaviour of tapered reinforced concrete beams in shear is poorly addressed in many design codes of practice; and second the construction of non-prismatic elements is often deemed to be complex and therefore expensive. As a result, fluid concrete tends to be cast into rigid orthogonal moulds. In doing so, designers fail to capitalise on its inherent ability to take up almost any shape.

The second concern has been addressed through research into the use of fabric formwork, which describes a method of construction for concrete elements in which rectangular sheets of fabric are used in lieu of steel or timber moulds. Originally used in the construction of underwater structures, fabric formwork allows complex shapes to be easily cast, thus facilitating the construction of optimised structures. The resulting forms have provided us with a new architectural language for concrete structures, Figure 1. Veenendaal *et al* [5] provide a comprehensive review of the history and applications of fabric formwork.

This paper reports on recent advances in the analysis and shear design of fabric formed concrete beams that have been made possible through the use of digital image correlation techniques applied using '*MatchID*' [6]. The shear behaviour of non-prismatic steel reinforced concrete beams is assessed, with some highlights of an extensive testing program analysed before recommendations and conclusions are presented.

Figure 1: *Fabric formed concrete. Curtain wall (left); Optimised beams (right).*

Shear behaviour

The shear behaviour of non-prismatic concrete structures has received limited attention. It is evident that a suitably inclined force in compression or tension may provide some resistance to shear, and Park and Paulay [7] suggest that the effective shear force in haunched beams without shear reinforcement should be given by Equation (1.1) (derived by considering the equilibrium of a tapered beam). This approach is cited in much of the available literature on tapered beams in shear [8-11].

$$V_{eff} = V - (M/z)(\tan\theta') \qquad (1.1)$$

Where the value of θ' *is positive in sections where the member depth increases in the direction of increasing moment;* V_{eff} *is the effective shear force on a section;* V *is the shear force on the section from the applied loads;* M *is the bending moment at a section;* z *is the lever arm between centres of tension and compression;* θ^1 *= angle of beam slope from the horizontal.*

In the steel reinforced section, cracks form when the principal tensile stress in the concrete exceeds its tensile capacity, and inclined cracks typically propagate from the tension face of the member towards the neutral axis as the applied loads are increased. In sections that taper towards their supports, it is imaginable that the interaction of these diagonal cracks with the path of the compression force that reaches the supports is perhaps more critical. Along with the contributing factors by which a reinforced concrete beam can carry shear, this is illustrated in Figure 2.

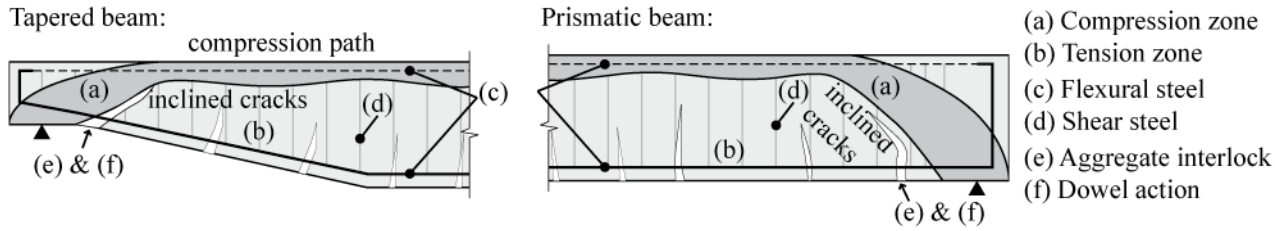

Figure 2: *Contributing factors to shear resistance in tapered and prismatic section.*

The shear behaviour of steel reinforced concrete is thus particularly important to understand in members of variable depth. Premature shear failures in optimised beams designed to fail in flexure using the provisions of BS 8110-1 [12] suggests that some codified methods may be unable to fully account for the shear behaviour of the tapering beam sections that are often found in fabric formed structures [13, 14].

Testing program

A testing program including thirteen steel reinforced tapered beams was undertaken in the preparation of this work. Three design approaches, denoted *EC2*, *CFP* and *STM* were used. Outlined briefly in Figure 3, the *EC2* method applies the provisions of BS EN 1992-1-1 [1]

(cl.6.2.1) where the inclined chord provides shear resistance (V_{td}). The *CFP* design applies the principles of the compressive force path method described in detail by Kotsovos and Pavlovic [15], in which the entire shear force is carried by the uncracked concrete in compression, while *STM* uses a strut and tie model in which the beam is imagined as a truss (Figure 3(right). The resulting range of taper geometries studied is illustrated in Figure 4. For the purposes of this paper, full analysis and results from only three of the beams is presented (2_EC2, 2_CFP and 2_STM). Each beam was tested in two arrangements (*V* and *M*, as shown in Figure 4), giving a total of six tests for which data is presented. The arrangement of the supports is such that in each test the tapered section has a shear span of 500mm and the span between supports is 2m.

CFP beams tested in setup *M* were designed to have a ductile flexural failure mode, while those tested in setup *V* were designed to have a shear-flexure failure. *EC2* beams tested in setup *V* were designed such that the flexural steel carries the entire shear force (V_{td} in Figure 3(left)); in setup *M* this contribution was ignored and designed transverse steel reinforcement was provided in accordance with the provisions of BS EN 1992-1-1 [1] (cl.6.2.3). *STM* beams tested in setup *M* had an additional end plate attached to the beam as anchorage; this was omitted in setup *V*.

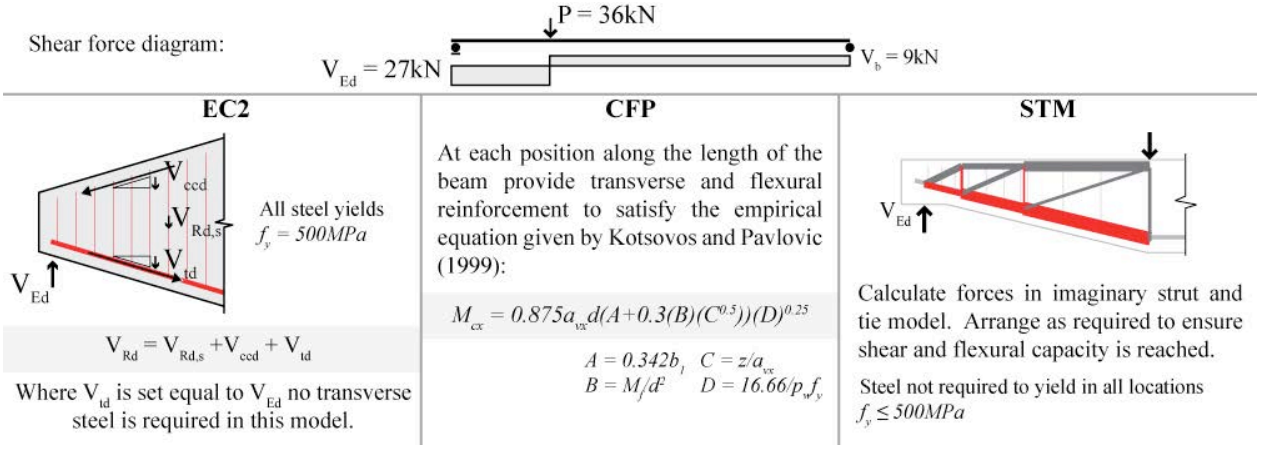

Figure 3: *Summary of load envelope (top) and the three design methods (bottom, left-right).*

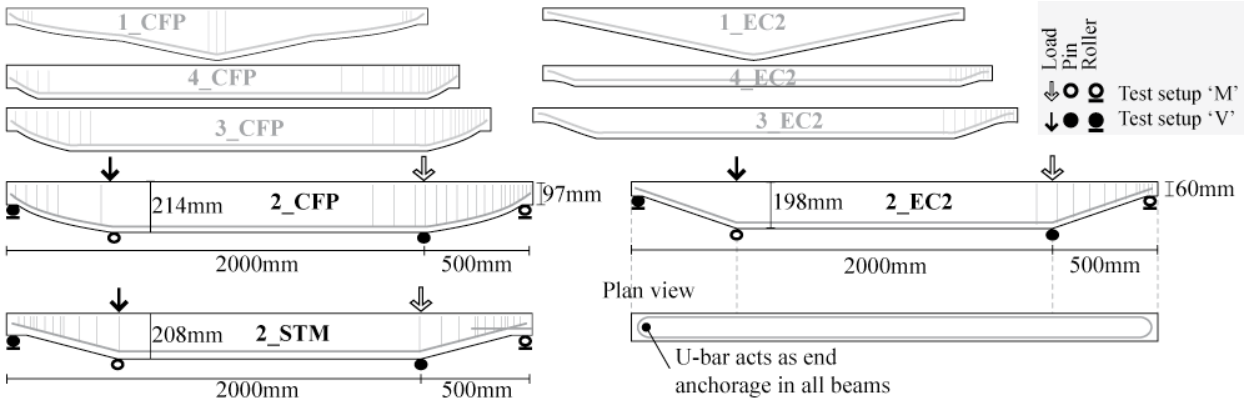

Figure 4: *Range of beam design geometries*

Each beam had a top breadth of 110mm and was reinforced on its tension face with two 10mm diameter high yield bars (yield strength, $f_y \geq 500$MPa). Where transverse reinforcement was used, these were 3mm diameter plain bars with $f_y \geq 500$MPa. All links were supported using 3mm bars in the compression zone, which are ignored for design purposes due to their minimal effect on flexural capacity. The design concrete strength was 40MPa, and cube tests taken prior to each test showed an average compressive strength of 38.7MPa (Standard Deviation = 0.68). All beams were cast in steel moulds, demoulded after 24 hours and tested after 14 days curing in laboratory conditions.

Monitoring

For the purposes of this test series, the tapered section of each beam was painted with a black and white speckled pattern (Figure 5(left)). Photographs were taken with a 16MP Canon SLR camera, using a 105mm lens placed 4m from the beam face. A second high-definition video camera was also used to record all the tests (Figure 5(right)). Conventional monitoring in the form of strain gauges and displacement transducers were also placed on the beams. Images were collected at each loading increment, and where ductile behaviour was recorded post-peak load, images were collected at increments of midspan displacement. All images were collected automatically using a computer.

Figure 5: *Example of speckled pattern (left); Digital image collection and test setup (right).*

Test Results

Each beam was loaded in 2kN increments. Cracking in the *EC2* beam series generally began at the support, before propagating towards the loading point. The *EC2* beams failed consistently in shear at less than the design load of 36kN. There was little recorded difference between the 'V' and 'M' type *EC2* beams, and in no cases was the longitudinal steel found to yield prior to failure, although this had been assumed in the design model.

In the *CFP* and *STM* series cracking began beneath the load point and propagated towards the support. In all cases, the longitudinal steel was found to yield prior to failure, and both *CFP* and *STM* type beams showed either crushing or shear-flexural failures at loads above their design predictions. A summary of the test results is provided in Table 1 and load-deflection results for the six tests considered in this paper are given in Figure 6.

Table 1: *Summary of all test results*

Beam	*Design maximum load, P (kN) [A]*	*Maximum load achieved in test (kN) [B]*	*Failure mode*	*[B] / [A]*
2_EC2_V	36.00	28.20	Shear	0.78
2_EC2_M	36.00	32.08	Shear	0.89
Average B/A				**0.84**
2_CFP_V	36.00	46.9	Shear-Flexure	1.30
2_CFP_M	36.00	48.6	Shear-Flexure	1.35
Average B/A				**1.33**
2_STM_V	36.00	41.81	Shear-Flexure	1.16
2_STM_M	36.00	41.45	Shear-Flexure	1.15
Average B/A				**1.16**

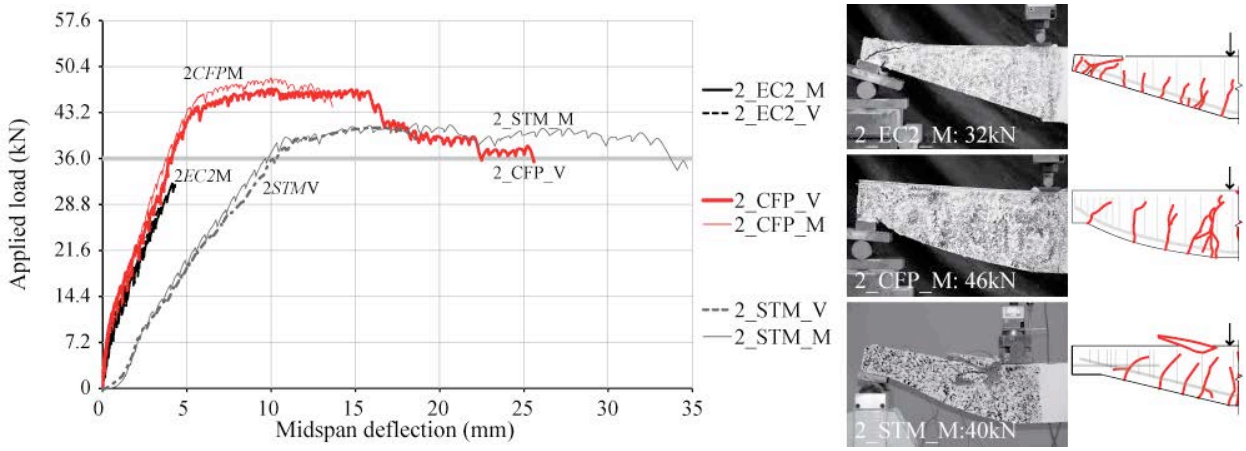

Figure 6: *Load-deflection results (l); Images and crack patterns at failure for 'M' type beams (r).*

Digital image correlation

Digital image correlation employs a static camera to take photos of a unique speckled pattern, which is then processed to determine displacement and strain distributions. Initial work to process the numerous collected images was undertaken using '*GeoPIV*', which uses normalised cross-correlation to calculate changes in a sequence of images [16, 17]. Limitations of this software led to the programming of a new script for use in the commercial software '*Digiflow*' [18] which proved enormously useful in obtaining initial results. The large image size (4752x3168 pixels) at each loading increment required considerable computing power to process, and a XX CPU was used for this purpose.

Whilst both GeoPIV and Digiflow provided excellent initial results, the final analysis was carried out using '*MatchID*', provided under a free license by the Catholic University College Ghent [6]. Using this program, the strains ε_{xx}, ε_{yy}, ε_1 and ε_2 were calculated for each beam. To save on computing time, the original photographs were reduced in size by 25% and converted to black and white tagged image format files. Calculations subsequently undertaken on both the original and reduced photographs revealed little advantage in using the full size image, and thus the smaller versions were used throughout the analysis.

Analysis

With data collected throughout the loading cycle, plots of the full behaviour of each beam can be made. This provides a new dimension of analysis to concrete beam behaviour, where steel strains and element displacements have previously been the most widely collected test data. An example of this is shown for one beam in Figure 9. Amendments to the MatchID program, suggested during this research, have resulted in the ability to set a single scale for all images, with the result that comparisons between the three sets of data can now easily be made. In the following, calculated strains ε_{xx}, ε_{yy}, ε_1 and ε_2 are presented (to the scale given in Figure 10). Of the two tests undertaken for each beam, only the '*M*' series results is presented due to space constraints. Following analysis using MatchID a comparison was first made between the strain distributions in of the beams at the load corresponding to the premature failure of Beam 2_EC2_M (32kN), which failed to reach the design load. This is shown in Figure 7. In Figure 8 a second comparison is made between the same beams at their respective peak loads (see Table 1).

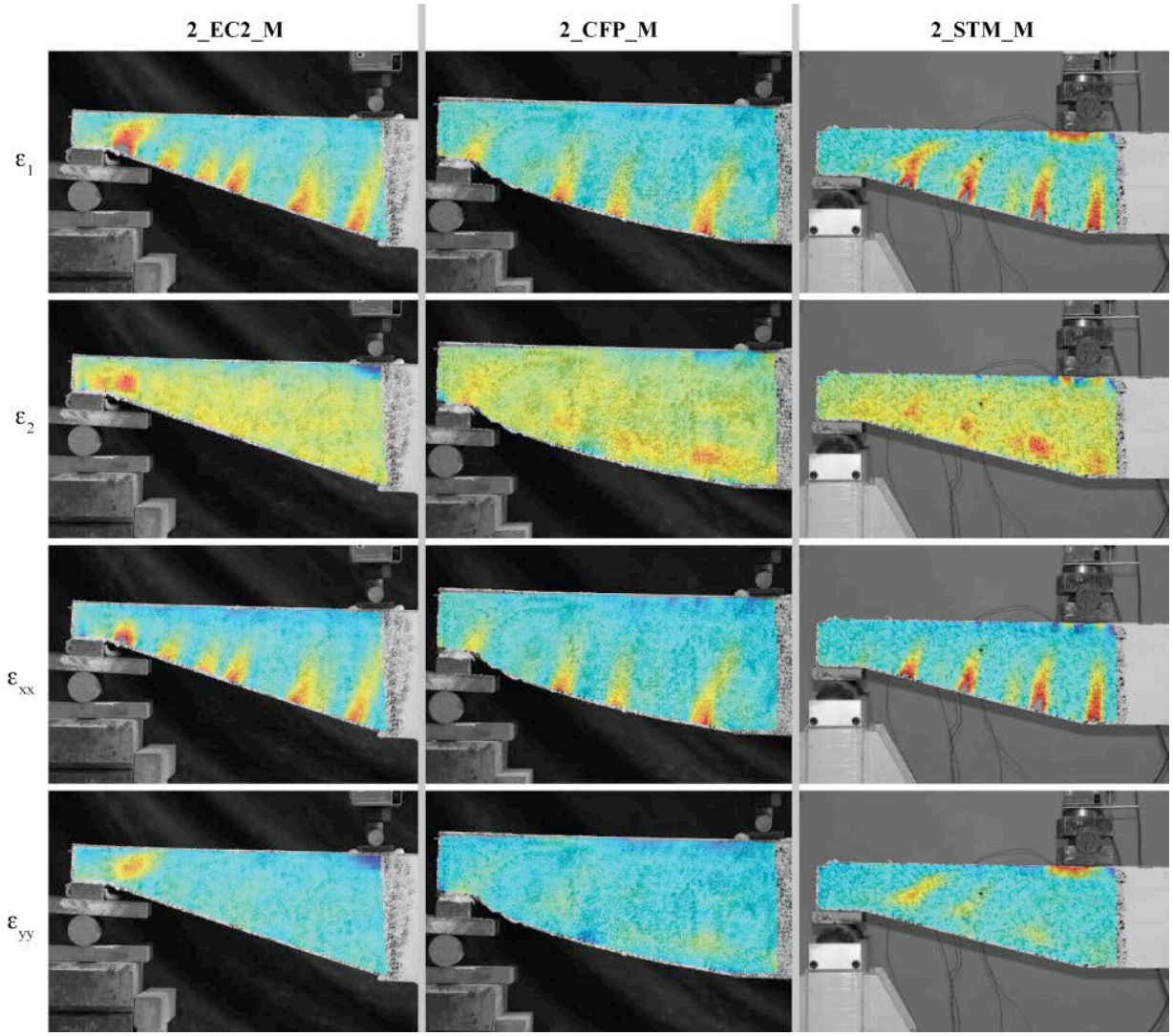

Figure 7: *Strain plots for 'M' beams, at the failure load of 2_EC2_M, 32kN.*

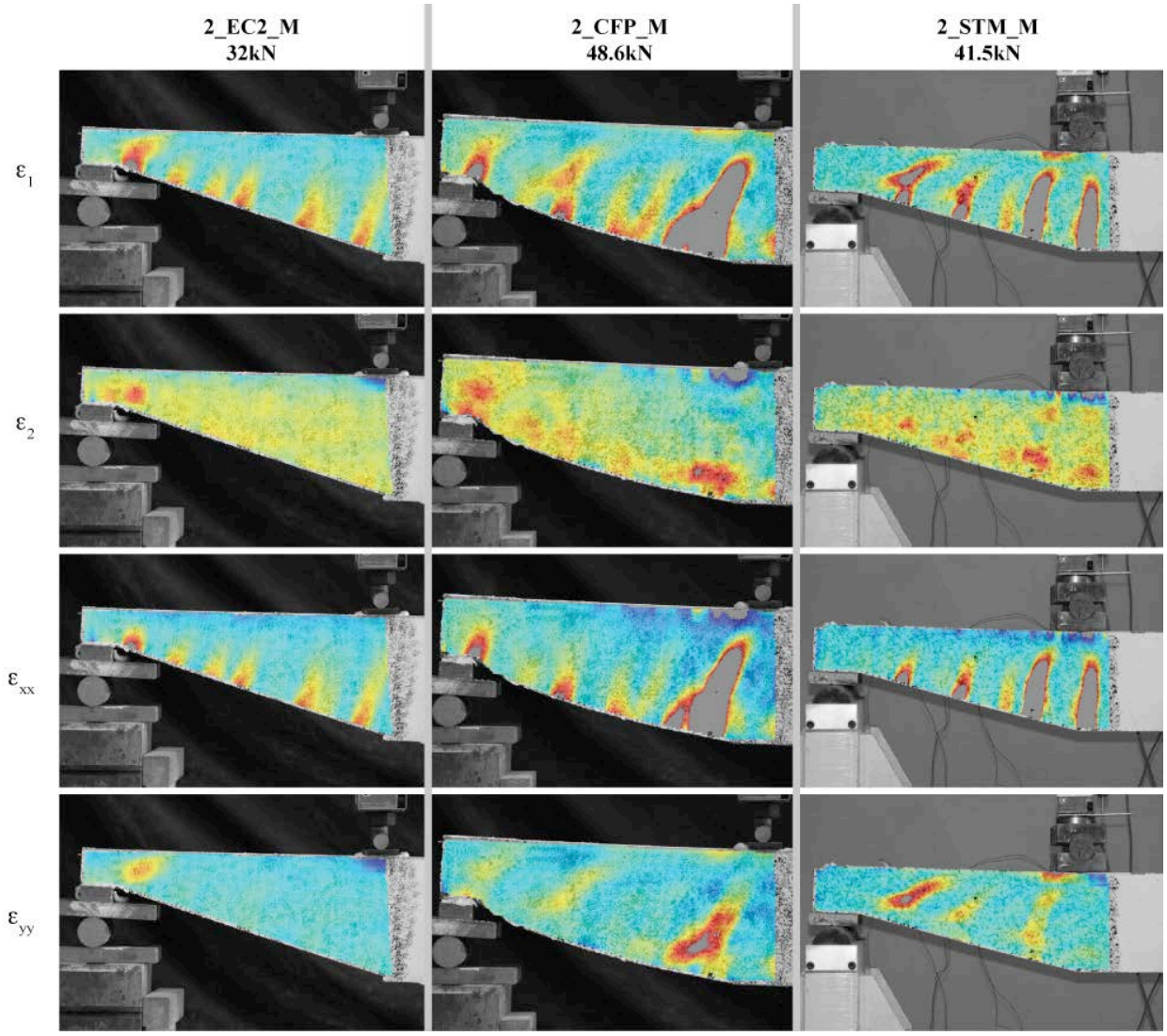

Figure 8: *Strain plots for 'M' beams, at their respective failure loads (noted above).*

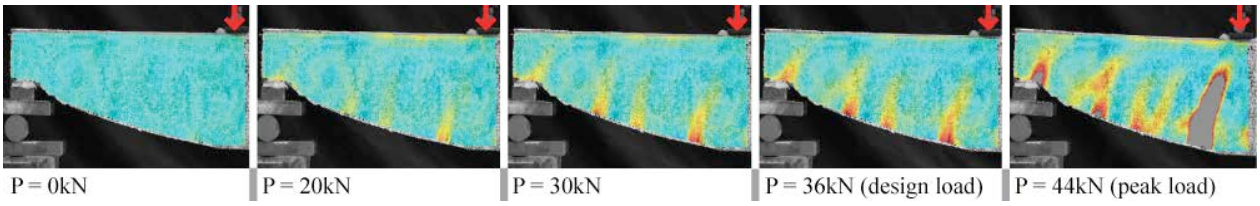

Figure 9: *Progression of strain plots through loading cycle for beam 2_CFP_V*

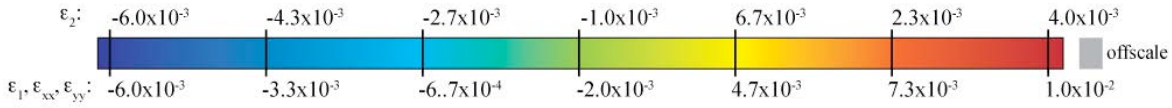

Figure 10: *Scale bar for PIV all results*

The *EC2* beams described above reached on average just 84% of their design load, while the *CFP* beams exceeded the design load by around 33% and the *STM* beams by 15%. The data presented above is just a sample of the total testing program, in which 24 tests were undertaken. In the full data set the *EC2* beams achieved on average just 58% of their design load, while the *CFP* and *STM* beams exceeded the design load by 20% and 10% respectively. The full data will be presented separately in a forthcoming journal paper.

In the *EC2* series, elements with transverse reinforcement (*M*) were found to behave almost identically to those without transverse reinforcement (*V*). It was proposed in the design model for *V* type beams that the flexural reinforcement would carry the entire shear force, and whilst this was not achieved (the beams failed to reach their design loads) the similarity in failure load between the *V* and *M* type beams suggests that the transverse reinforcement present in the *M* type beams was ineffectively placed to increase the shear capacity of the section. Further exploration of the effective placement of the transverse reinforcement is discussed in [15].

The advantage of the *CFP* and *STM* models is shown in the DIC results of Figure 7. At its failure load of 32kN, Beam *2_EC2_M* shows a concentrations of ε_{xx} strain (crack locations) and a 'hot spot' of vertical strain at the support. At the same load, the *CFP* beam has fewer cracks and the ε_{yy} strains do not peak at the support. The *STM* beam shows a similar behaviour, with well-spaced cracking and a small peak of vertical strain occurring on an inclined line running away from the support. This resulted in cracking, but not premature failure.

At their respective failure loads (Figure 8) the *CFP* beam has its peak ε_{xx} and ε_{yy} strains beneath the loading point, which has led to the flexural failure mode illustrated in Figure 6. The *STM* beam shows peak ε_{yy} strains at the support, but there also exist deep flexural cracking and high compression beneath the load point, both of which contributed to a similar flexural failure mode (Figure 6). The stress distributions at failure are quite different to that seen in Beam *EC2*, where high strains at the narrow support appear to govern the failure load, even in sections with designed transverse reinforcement. In the deeper support zone of the *CFP* and *STM* beams the strain distribution revealed by the DIC supports the design method as being more appropriate for tapered beams in shear.

The *EC2* design method assumes that the steel has yielded; yet this is not seen in the test data. In contrast, the *STM* model (which does not require the steel to yield) is able to rely on plasticity because the beam is designed to have a ductile flexural failure mode and so becomes a self-fulfilling prophecy in which a ductile failure is achieved. By contrast the *EC2* method, which assumes all the steel yields, becomes a vicious circle leading to premature shear failures.

Conclusions

Conservative results from both the *CFP* and *STM* beam design methods, supported by DIC data showing how the internal strain distribution is altered in these design methods, suggests that they are better able to model the behaviour of tapered beams in shear. In light of the results presented for the *EC2* beam series, it is recommended that tapered beams do not rely entirely on the contribution of their flexural steel to the shear capacity (i.e. V_{td} (Figure 3(left)) should not

comprise the full value of V_{Rd}) until further guidance can be determined. The application of both STM and CFP method has been shown to be successful, and a fuller description of the design model, along with DIC information and strain direction plots for the remaining tests not discussed in this paper is to be presented in a forthcoming journal paper.

References

[1] BS EN 1992-1-1:2004, *Eurocode 2: Design of concrete structures - Part 1-1: General rules and rules for buildings*, BSI.

[2] Wri, *Carbon Dioxide Emissions by Source 2005*, Earthtrends Data Tables: Climate and Atmosphere, 2005

[3] Bis, *ESTIMATING THE AMOUNT OF CO2 EMISSIONS THAT THE CONSTRUCTION INDUSTRY CAN INFLUENCE: Supporting material for the Low Carbon Construction IGT Report*, BIS (Department for Business Innovation and Skills), 2010

[4] Thirion, C., *Putting the material in the right place: the role of material-efficiency in reducing the environmental impact of building structures*, Department of Civil, Environmental and Geomatic Engineering, University College London, MRes Thesis, 2010

[5] Veenendaal, D., West, M. and Block, P., History and overview of fabric formwork: using fabrics for concrete casting, Structural Concrete, **12**, 164-177 (2011).

[6] Lava, P. and Debruyne, D., *MatchID*, Catholic University College Ghent, 2010

[7] Park, R., Paulay, T., *Reinforced concrete structures* (John Wiley and Sons, 1975)

[8] Macleod, I. A. and Houmsi, A., Shear strength of haunched beams without shear reinforcement, ACI Structural Journal, **91**, 79-89 (1994).

[9] El-Niema, E. I., Investigation of haunched concrete T-Beams under shear, ASCE, **114**, 917-930 (1988).

[10] Debaiky, S. Y. and Elneima, E. I., Behavior and Strength of Reinforced Concrete Haunched Beams in Shear, ACI Structural Journal, **79**, 184-194 (1982).

[11] Guyon, Y., *Prestressed Concrete* (Contractors Record and Municipal Engineering, 1953)

[12] BS 8110-1:1997, *Structural use of concrete - Part 1: Code of practice for design and construction*,

[13] Garbett, J., *Bone growth analogy for optimising flexibly fomed concrete beams*, Department for Architecture and Civil Engineering, University of Bath, MEng Thesis, 2008

[14] Bailiss, J., *Fabric-formed concrete beams: Design and analysis*, Department of Architecture and Civil Engineering, University of Bath, MEng Thesis, 2006

[15] Kotsovos, M. D. and Pavlovic, M. N., *Ultimate limit state design of concrete structures, a new approach.* (Thomas Telford, 1999)

[16] White, D. J., Take, W. A. and Bolton, M. D., Measuring soil deformation in geotechnical models using digital images and PIV analysis. in *Proceedings of the 10th International Conference on Computer Methods and Advances in Geomechanics*. Tucson, Arizona, 2001

[17] Bisby, L., Take, W. A. and Caspary, A., Quantifying strain variation in FRP confined concrete using digital image correlation: Proof of concept and initial results in *Asia Pacific Conference on FRP in Structures*, 2007

[18] Dalziel, S., *Digiflow*, Department of Applied Mathematics and Theoretical Physics (DAMPT), 2011